A novel approach for damage assessment in adhesively bonded composite joints using backface strain technique

Original
A novel approach for damage assessment in adhesively bonded composite joints using backface strain technique / Abbasi, M., Ciardiello, R., Goglio, L.. - In: COMPOSITES. PART B, ENGINEERING. - ISSN 1359-8368. - 286:(2024), pp. 1-16. [10.1016/j.compositesb.2024.111766]

Publisher:
ELSEVIER

Published
DOI:10.1016/j.compositesb.2024.111766

A Novel Approach for Damage Assessment in Adhesively Bonded Composite Joints using Backface Strain Technique

M. Abbasi[12], R. Ciardiello[12], L. Goglio[12]

[1] Department of Mechanical and Aerospace Engineering, Politecnico di Torino (IT)
[2] J-TECH@POLITO. Advanced Joining Technologies, Politecnico di Torino (IT)
* Correspondence: mohammad.abbasi@polito.it

Abstract

In this study, the backface strain (BFS) is measured by both digital image correlation (DIC) and fiber optic sensors (FOS) to detect the crack initiation and propagation in adhesively bonded composite single-lap joints (SLJ). BFS measures the resultant strain deriving from the positive strain, due to tensile load, and negative strain related to the bending moment. A point, called zero-strain point (ZSP), can be detected on the substrate surface of SLJ due to the concurrent effect of these positive and negative strains. The experimental activity shows that the value of the ZSP changes when the crack starts to propagate. Thus, this point can be used to monitor the service conditions of adhesive joints. The effect of joint dimensions on the position of the ZSP is investigated when the joint is subjected to quasi-static loading. In addition, the applicability of the method is investigated under a cyclic loading condition. The work shows that the ZSP can be used as an index to monitor joint healthiness. Furthermore, FOSs can be used for an in-situ monitoring of the joint.

Keywords: Composites Single-Lap Joint (SLJ), Digital Image Correlation (DIC), Fiber Optic Sensor (FOS), Backface Strain (BFS), Structural Health Monitoring (SHM)

1. Introduction

In the past decades, it has been seen that composite materials have been increasingly used as alternatives for metals, mainly due to their good mechanical properties, the possibility to fabricate complex geometries, lightweight and high resistance against corrosion[1,2]. Consequently, this fast growth of composite applications in different industries like automotive, aerospace, civil and marine engineering has prompted to use reliable joining methods to connect small or large components [3,4]. Up to now, mechanical fastening like bolts and rivets, welding and adhesive bonding are widely used techniques to join composite materials [5–7]. Adhesive bonded joints offer significant advantages over traditional mechanical joints, such as reduced weight, lower fabrication costs, improved damage tolerance, and the ability to join dissimilar materials without the corrosion concerns related to metal fasteners. Due to these benefits, these joints have found extensive applications in various industries including aerospace and automotive[1,3,8,9]. Therefore, it is important to fully understand the mechanical behavior of adhesive joints to apply proper strategies for monitoring these joints. The adhesives are expected to fail before composite substrates during the structure service life because they present lower mechanical properties. As a result, although there are also methods to improve the joints adhesive joints [10] they are designed with conservative safety margins [9,11]. Thus, it can be crucial in critical applications which demand high safety to develop non-destructive techniques that allow structural health monitoring (SHM) of the applications by warning at the initial stage of damage or providing reliable information about joint healthiness throughout service life. This enhances safety and reduces maintenance costs for those applications that need high reliability [12,13], and allows joint repair or replacement, when necessary, as well.

Various technologies and methods have been used to monitor the damage in composite joints [14–22] among which Digital Image Correlation (DIC) [23,24], and Fiber Optic Sensors (FOS) [25–28] were used in the present work. Fiber Bragg Grating (FBG) sensors are the most popular FOS, which work by etching micro-structure brag gratings inside an optical fiber core, reflecting a specific light wavelength [29]. This wavelength changes when an FBG is subjected to external mechanical or thermal load, which allows accurate measuring of strain. Due to the small size, FBGs might be embedded in the joint, but this may affect the mechanical properties of the specimens. DIC is a non-contact method which can inspect large areas based on the images acquired by high-frequency and resolution cameras [30]. DIC works based on comparing pixel by pixel of each acquired image with the previous image or a chosen reference image to measure the surface displacement and consequently the strain in the specimen. The drawbacks of the DIC are the difficulties while preparing the samples, limited damage type detection, extensive data acquisition and the impossibility of using it as an SHM methodology.

Backface strain (BFS) measurement technique that could be used as an NDT method was introduced in 1986 by Abe and Satoh [31] to study crack formation in spot-welded joints. As it is obvious from the method’s name, the first step is to measure the strain on the back surface of the specimen using one or more approaches. This technique has been applied to adhesively bonded joints, resulting in numerous investigations [12,13,31–35] that aim to efficiently detect adhesive joint damage. The BFS measurement method is particularly effective for evaluating the presence of hazardous cracks [12,13]. Usually, this method involves placing strain gauges on the external surface of the bonded joint, known as the backface. Zhang et al. [13] used a measuring point by installing strain gauges at the overlap's end, focusing on the increased bend caused by cracks. Solana et al. [33] used the BFS by measuring the strain on the backface by using strain gauges and monitoring the ones with the largest strain gradient. Considering the BFS method, many researchers tried to monitor the adhesively bonded SLJs damage by placing strain gauges on the joints where stress concentration is high [12,13,33]. However, establishing the optimal location for these gauges is challenging due to the mixed-mode nature of SLJs as a result of their geometry, in particular with the inhomogeneous structure of composite materials. In composite materials, the back faces could be influenced by the size of the adopted measuring system in connection with the size of the microstructure of the constituents of the materials (fiber or tow sizes). As shown by Boursier et al. [36], the size and location of the strain gauges highly influence the measure of the deformation which can lead to values of the elastic properties that are 50% higher compared to the reference value. Different works[37,38] attempted to use the BFS technique, employing arrays of strain sensors, to monitor crack propagation in SLJs and detect strains in different positions within composite SLJs. Moreover, there is the possibility of embedding sensors within composite laminates closer to the crack [39]. Therefore, FBG sensors were attached on the specimen internal surface to estimate how they would behave when placed in the laminate. This allowed the researchers to spot and track crack growth in a bonded joint during fatigue testing. In SLJs, crack initiation and propagation can be monitored by detecting the position of the BFS profile peak [13]. The position of this strain profile peak has been confirmed to closely correspond with the crack tip location [12]. The correlation between the crack front and the BFS peak location in SLJs depends on factors like adhesive fillet presence, materials used, and substrate mechanical properties. Preisler et al. [32] employed the zero-strain point within the region exhibiting the most significant change in longitudinal strain for monitoring structural damage. ZSP is a point where the strain is zero due to the concurrent effect of tensile and bending strain. Under normal, undamaged conditions, there is no longitudinal strain present, independently of the applied load.

Different parameters are proven to have a noticeable effect on the general mechanical behavior of SLJs [40–42]. These parameters include substrate materials, adhesive type [1,41], overlap length [43], adhesive thickness [44,45], joint width [41,42,46], fillets at the edges [47], and surface treatment [48]. Regarding the bonding area dimensions and adhesive types, previous works mainly investigated the effect of these parameters on properties like peak force, elongation, shear stress, normal stress, peel stress [41,42]. Two main adhesive types, polyurethane-based and epoxy-based, have been extensively studied in different sectors including the automobile and aerospace industries. Polyurethane adhesives are popular due to their capacity to withstand larger deformations, and their sealing ability [49,50]. Epoxy adhesives are of interest because of their ability to join similar and dissimilar materials, as well as having good fatigue properties, and resistance against impact [51–53].

This research activity focuses on monitoring the crack initiation and following its propagation in composite single-lap joints with different bonding area dimensions subjected to quasi-static and cyclic loading. Therefore, a large campaign of tests was carried out using DIC to monitor the deformation of the backface of the SLJ. The results were also validated by fiber optic sensors due to their ability. As a result, zero-strain ZSP was identified on the backface of the joint. The monitoring of this point provides enough information to analyze the behavior of SLJs and the health condition of SLJs over the service life. Moreover, the effect of bonding area geometry including Overlap length (L), Joint width (W) and Substrate thickness (T) on the position on ZSP was investigated. This comprehensive research activity on the effects of different parameters on ZSP position using the DIC and fiber optic sensors allowed an elaboration of a strategy to monitor SLJ in both online and offline modes. Finally, having the methodology confirmed, it is proposed to use it with fiber optic sensors in real applications. The work addresses different open points in the literature. Realistic thicknesses and sizes of the composite substrates were used to assess any limitation of the ZSP technique. The activity is focused on composite materials which present two phases, matrix and resin, to evaluate any possible effect and limitation of the adopted technique. Cyclic loading was used to demonstrate that the ZSP can detect the damage and that the change of ZSP is not solely related to the effect of the overall damage. Further, a comparison of the strains between fiber optic sensors and DIC techniques shows that the optics sensors can be used for SHM applications. The optical sensors, compared to strain gauges offer the possibility to continuously measure the strain along a line while strain gauges can just provide local information that is more complex to be analyzed and installed.

2. Experimentation

2.1. Materials and design of experiments

A bi-component polyurethane adhesive called ADEKIT A236/H6236, made by the Sika (CH), was utilized in this investigation. This glue may be used in a variety of applications and sectors, including transportation, marine, automotive, and aerospace, according to the technical data sheet. The mechanical properties of this adhesive were studied and reported in [41,42] as given in Table 1. On the other hand, a carbon fiber/epoxy prepreg weave, XPREG XC130, was used for the substrates. This prepreg presents a real weight of 210 grams per square meter (gsm) and it is a 3k reinforcement which combines a high strength TR30S fiber with a 2x2 twill weave (the fibers orientation is 0/90). The main mechanical characteristics of this prepreg are given in Table 2.

Table 1 Mechanical properties of adhesive (Polyurethane ADEKIT A 236/H 6236) [41,42]

E (MPa)	278
SIG ultimate (MPa)	13
Elongation (%)	22
Density	1.35

Table 2 Mechanical properties of the carbon fiber composite material [54,55].

	Mean Value
Density (kg/m^3)	1450
Poisson’s ratio	0.12
Longitudinal modulus (MPa)	58,000
Longitudinal tensile strength (MPa)	440

Longitudinal compressive strength (MPa)	453
Longitudinal compressive ultimate strain	0.096

To investigate the effects of bonding area dimensions on the mechanical behavior of the joints, including damage initiation and propagation, samples were manufactured with various adherend thicknesses (T1 = 0.88 mm, T2 = 1.76 mm, T3 = 3.52 mm), joint widths (W1 = 10 mm, W2 = 20 mm, W3 = 30 mm), and overlap lengths (L1 = 10 mm, L2 = 20 mm). Figure 1 shows the SLJs sketch with the considered dimensions. The area between the loaded edge and non-loaded edge on the outer face of the substrate is called backface. These three parameters were also used to name the specimens. For example, L1W2T3 represents a specimen with an overlap length of L1, a joint width of W2, and an adherend thickness of T3. A Design of Experiment based on these parameters is provided in Table 3, with three repetitions for each sample. The adhesive thickness was $t_{adhesive}$=1.10 mm, as recommended by the datasheet for adhesive. A fixture was used to align the joints, employing Teflon spacers to achieve the desired thickness.

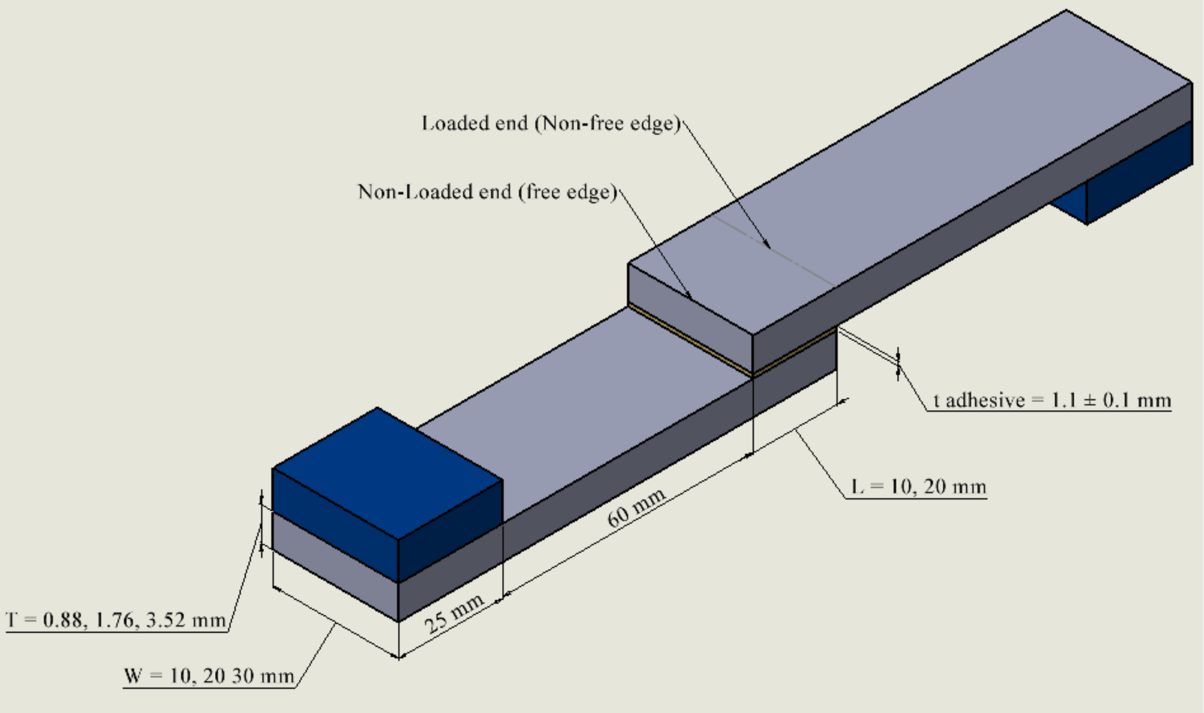

Figure 1. SLJ geometry (L: overlap length, W: joint width, T: substrate thickness, and $t_{adhesive}$: adhesive thickness)

Table 3. SLJ design of experiments [41,42]

Parameters		T1 (0.88mm)	T2 (1.76mm)	T3 (3.52mm)
L1 (10mm)	W1 (10mm)	L1W1T1	L1W1T2	L1W1T3
	W2 (20mm)	L1W2T1	L1W2T2	L1W2T3
	W3 (30mm)	L1W3T1	L1W3T2	L1W3T3
L2 (20mm)	W1 (10mm)	L2W1T1	L2W1T2	L2W1T3
	W2 (20mm)	L2W2T1	L2W2T2	L2W2T3
	W3 (30mm)	L2W3T1	L2W3T2	L2W3T3

2.2. SLJ specimen manufacturing, FOS installation, and speckle pattern for DIC

The preparation of the SLJs followed the same procedure detailed in papers published by the same authors[41,42]. In brief, laminates with varying numbers of layers (2, 4, and 8 layers) were made using hand layup method, vacuumed, cured in an oven, and then, cut into the desired dimensions. The surface preparation of the substrates was conducted by abrading the joint area with sandpaper and cleaning it with acetone. The joints were assembled using a handmade mold to align the joint, and the adhesive was cured in two steps. First, it was cured at ambient temperature, followed by a post-curing process in an oven at 70°C for 16 hours, as specified in the manufacturer's datasheet. Excess adhesive was removed after curing to prevent increased and uncontrollable joint stiffness and strength. To obtain the desired adhesive thickness Teflon spacers with the same thickness were used. Moreover, to have good control of the adhesive thickness throughout the overlap length, a weight was applied on the upper substrate in a way that covers all the bonding area. Moreover, a set distance of 85 mm from both ends of the bonding area is also thought to separate the start of the bonding region from the end of SLJ (Table 1).

When the SLJ samples were prepared (Figure *2*a), optical fibers were installed on both outer surfaces of the joint area, i.e., outer surfaces of substrates. Both outer faces on both sides of the SLJs were considered to observe if this fiber could measure the same deformations on both outer sides (faces) of the joints. This optical fiber is installed in a way that it has two lines of attachment on each side of the joints with overlap length size. Therefore, a total of 4 lines (parts) from a single optical fiber were attached to the SLJ outer faces in the overlap direction. This lets us to have the information about the deformation on two lines on each side. Figure 2b shows the installed fiber only on one surface of the joint. To ensure the fiber is straight and without any bends, they are maintained in a slightly tensile position and attached to the joint area using an isocyanate fast glue.

Finally, the specimens were painted to be recognizable by the Digital Image Correlation (DIC) tool. For this purpose, the bonding area is first painted with white color and then a speckle pattern is produced by spraying the black color as random points. It is tried to make the pattern randomly formed with black and white points considering an approximate ratio of 1 (Figure 2c). At the end, two tabs of 25 mm were applied in the clamping area, as shown in Figure 1, to avoid misalignment while applying the load.

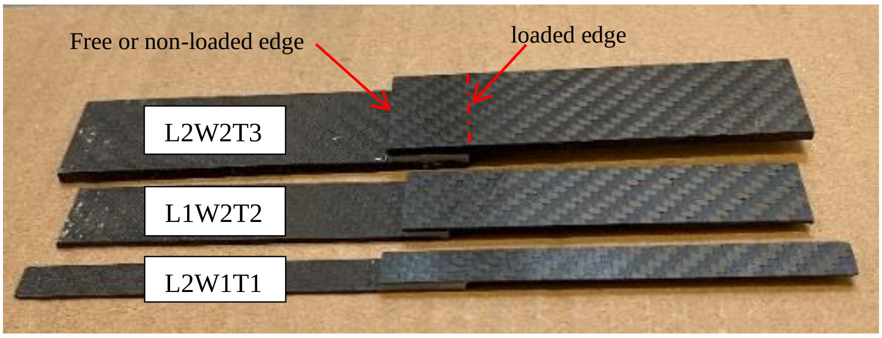

a)

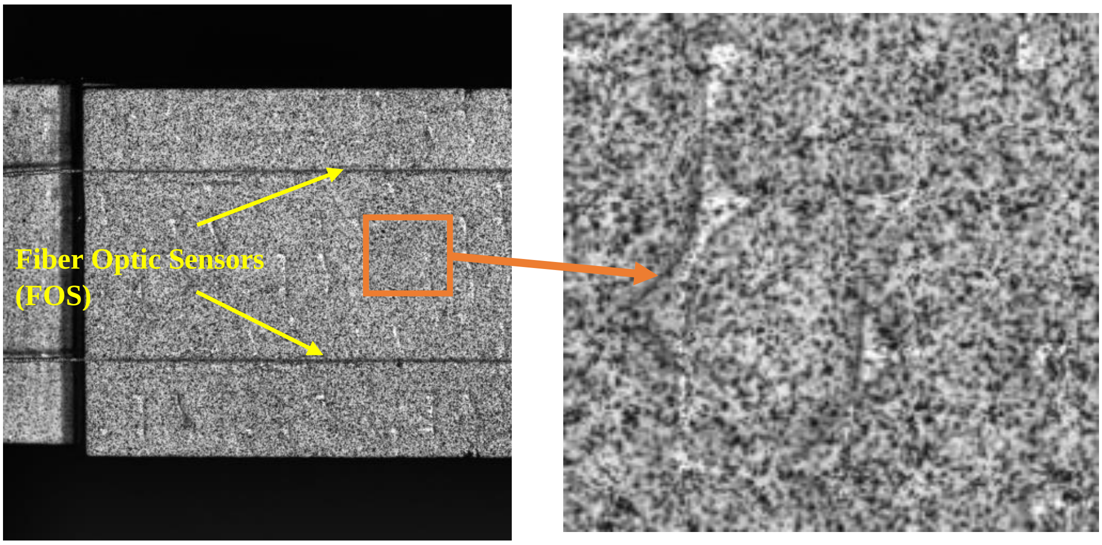

b) c)

Figure 2. Specimen preparation; a) prepared SLJs; b) SLJ with optical fibers (the one installed on the surface in front of DIC); c) pattern for DIC.

2.3. Test apparatus:

Tests were performed using servo-hydraulic Instron (Norwood, MA, USA) machine 8801 at a crosshead velocity of 5 mm/min. The test apparatus is shown in Figure 3. In addition, to observe and measure the displacement contours on the surface of the SLJs a Digital Image Correlation (DIC) tool from Correlated Solution (Columbia, SC, USA) was used in 3D mode. The lenses were of type Rodagon Smart Focus 80mm. The image acquisition was done by VIC-Snap software at a rate of 20 Hz which provides enough detailed data from each test. Further, DIC and Instron were synchronized to correlate the recorded load and crosshead displacement with each image. To minimize the processing time and the amount of data collected, making the correlation analysis feasible, it was required to restrict the frame that the software processes to a smaller area of interest surrounding the specimen. The software generates a rectangular array of subsets inside the area of interest during this operation. Subsets are square portions of the picture, spaced by the same distance (the step size) both in vertical and horizontal directions. Here, the subset size is 47 pixels and the subset spacing is 5 pixels. Finally, a strain acquisition system, LUNA Odisi 6000 system (Virginia, USA), that uses Fiber Optic Sensors (FOS) was used to simultaneously acquire the strain. The LUNA system works on the Rayleigh backscattering effect. The presence of impurities reflects the light travelling along the fiber, thus allowing continuous measurement of the strain [36]. This system takes advantage of high-definition optical fiber sensors and can provide thousands of strain and temperature measurements per meter for each fiber. The optical fibers manufactured by ThorLabs (Newton, New Jersey, USA) have been used in these tests. Gauge pitch is the distance between two successive acquisition points in the optical fiber length. The smallest resolution possible with the employed optical fiber in this study is a gauge pitch of 0.65 mm, and this value was adopted. Thus, it is possible to have 30-31 strain sensors along an overlap of 20 mm considering the used gauge pitch. This is not possible by using strain gauges, because of the size, neither with Bragg's optical fibers that use grating lengths of 1 or 3.5 mm. Another reason for using the optical fiber is that contrary to the DIC, the optical fibers can be installed on a real component, e.g., car parts, to provide the active and in-situ measurement of the strain.

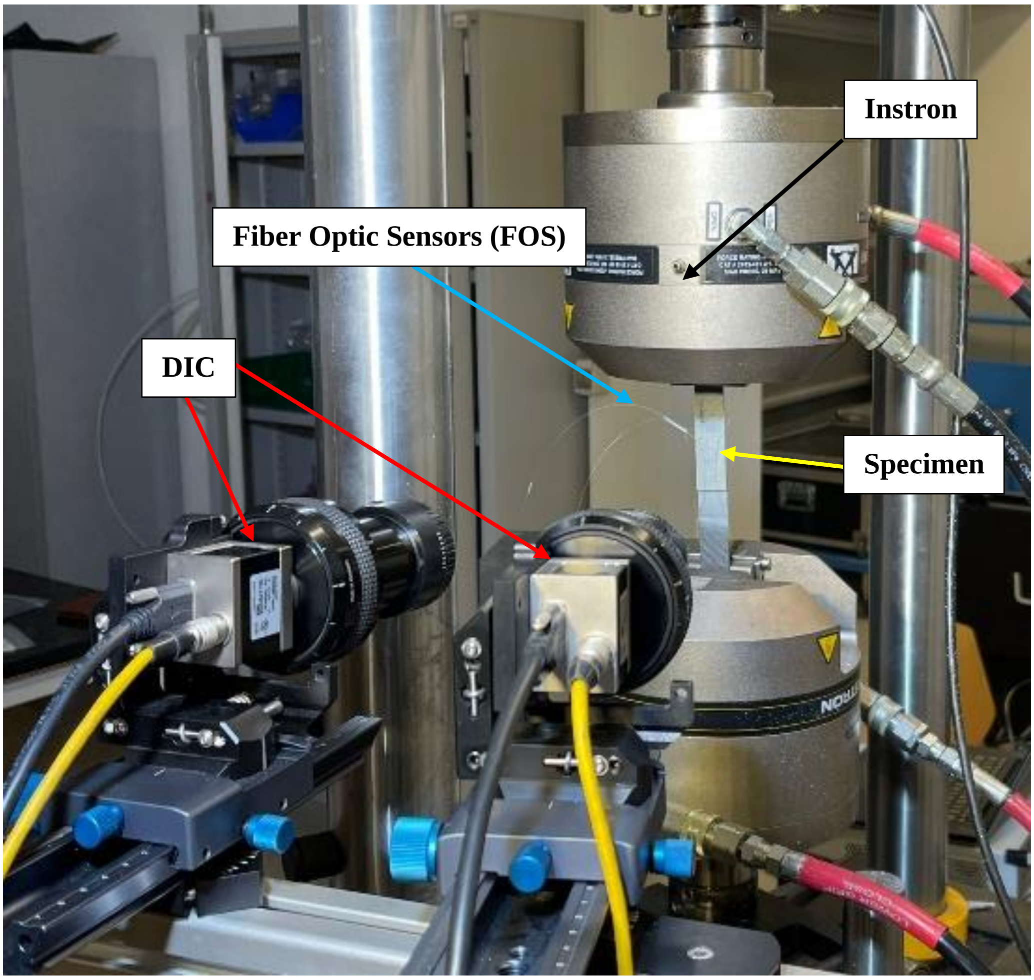

Figure 3 Test setup

3. Results and discussion

3.1. General response of the joints under tensile loading

Based on the test campaign that has been carried out in this study it is possible also to analyze how joint dimensions can affect the response of a single lap joint. The effects of each parameter on joint response including, peak load, displacement at peak load, adherend normal stress, adhesive shear and peeling stresses are already discussed in detail in previous publications [41,42]. The tests done for this study also confirm the results obtained in [41,42]. Three samples of each configuration mentioned in Table 3 were tested. Each configuration presented good repeatability. For the sake of brevity, one out of three curves are shown in Figure 4a. Moreover, Figure 4b, and c, shows the scatter for the peak force (F) in relation to the displacement at peak load (d). In Figure 4b, and c, the substrate thicknesses are represented by three different colors blue, red and yellow colors for T1, T2 and T3, respectively. The scatter is very limited for these types of tests, and the averaged values for W1, W2 and W3 are shown by the symbols solid circle, cross, and empty square, respectively. The values in the in Figure 4 show that all three parameters (L, W, and T) significantly influence the peak force and joint stiffness (the slope of the initial linear part of the load-displacement curve). The larger the bonding area the higher the peak force and the joint stiffness. The analysis of data in Figure 4 and all the repetition of the tests show that W is more influential than L and L is more influential than T on the load capacity of the joints. However, the effect of W on joint stiffness is greater than the effects of L and T. Moreover, after the test, specimens were carefully inspected and different types of damages including adhesive, cohesive, thin layer cohesive and mixed mode were observed as shown in Figure 5. According to [41,42] increasing the thickness of the substrate leads to a more uniform distribution of shear and peel stresses and a reduction of the peaks in the overlap ends. The adhesive in the center of the joint is compressed due to locally negative peel stress, and this compression is more pronounced in joints with thicker substrates. Therefore, the thicker the substrate the more cohesive the damage surface was.

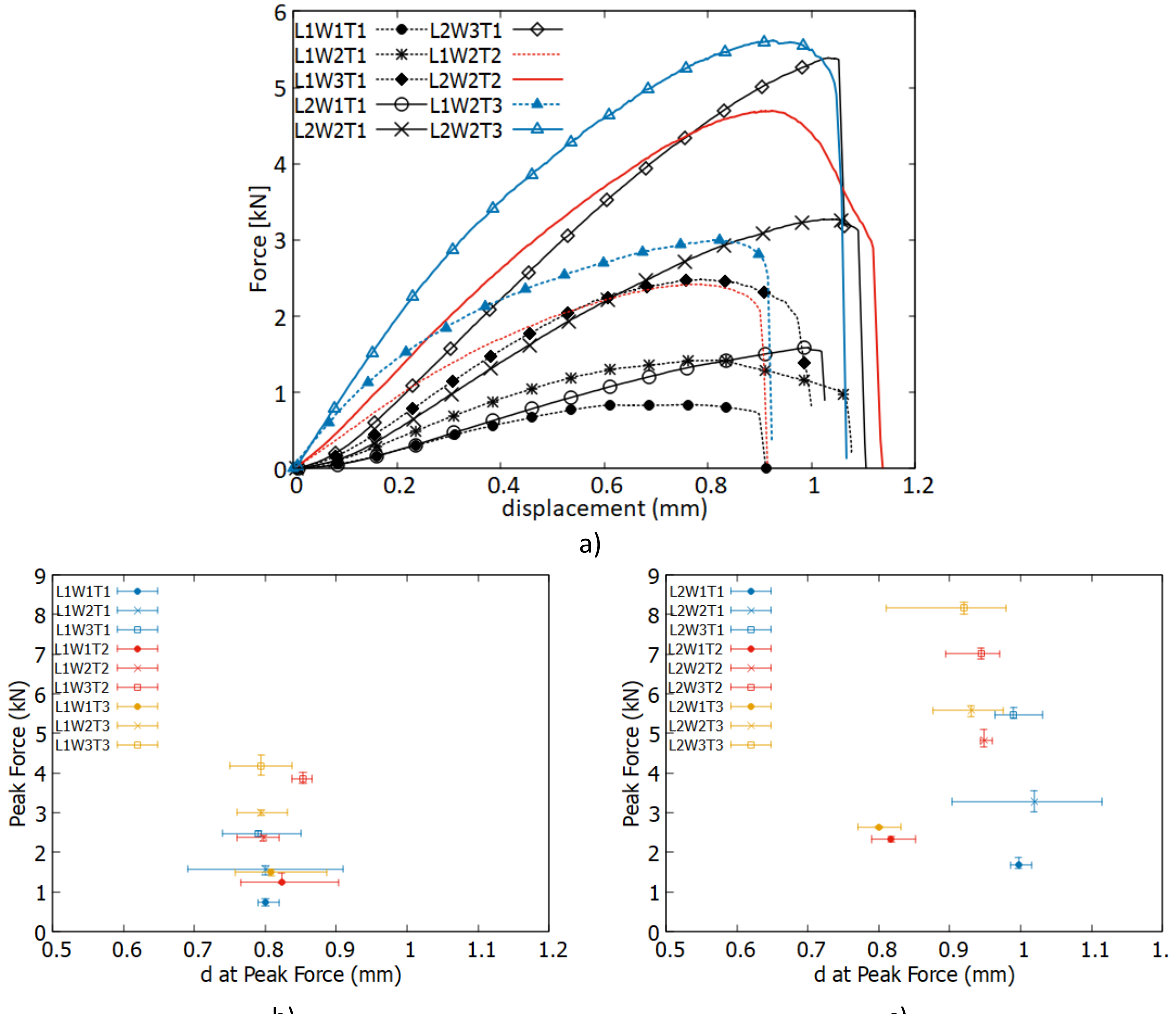

a)

b)

c)

Figure 4. Tensile response of the joints. a) Load-displacement curves all the specimens, b) scatter for samples with overlap L1, c) scatter for samples with overlap L2

L2W2T3 L1W2T2 L1W3T1

Figure 5 Failure surfaces of the specimens after the test a) L2W2Tb) L2W2T c) L1W3T

3.2. Definition of Zero-Strain Point (ZSP) using DIC

Generally, SLJs undergo a mixed-mode loading mainly due to the geometry and the eccentricity of the tensile load as shown in Figure 6. As a result, the specimens also experience bending moment, shear and peel stresses. The tensile loading causes positive strain in the substrates whilst the bending moment makes the substrates' outer face (backface) experience mainly a negative strain. The concurrent effects of these two types of strains on the overlap length will result in a point on the external surface (backface) of the substrate where the strain is zero. This point is called Zero-Strain Point (ZSP). The behavior and importance of ZSP is described using Figure 7 as follows.

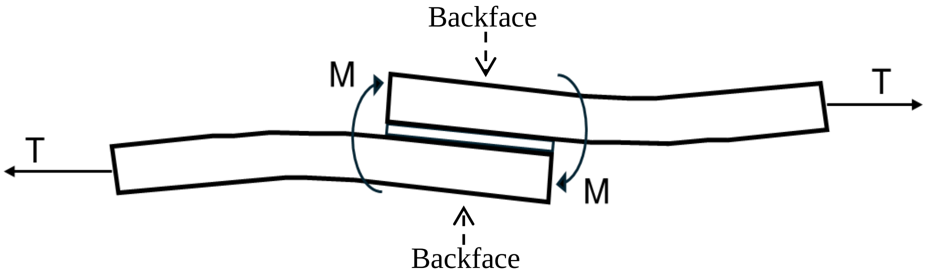

Figure 6 schematic of load eccentricity on SLJ.

Figure 7a,b,c, and d show, how the ZSP works for the specimen L2W1T1, taken as an example. In this specimen, the overlap length is 20 mm, the substrate thickness is 0.88 mm, and the joint width is 10 mm. After processing the images using VIC-3D software the strain contour map is shown over the overlap length in Figure 7a. Larger positive strain values have been found in the middle area of the joint (reddish contour) whilst negative values are observed in the vicinity of the joint edges. As can be seen in Figure 7a, different points along the overlap length have been chosen to monitor the strain history. Each point is the average of all the strain values over the joint width, e.g., the black point is the average of all strain values on the dashed yellow line. Therefore, each point is a representative of all the points with different positions on the joint width while they have the same position on the overlap length. Afterwards, the strain history for these points is shown in Figure 7b. Most of the points experienced either positive or negative strain from the beginning of the test. There are only a few points very close to each other in which the strain is zero and remains zero up to a certain time, that is, to a certain load level. Those points are the candidates for ZSP.

Another way to visualize the ZSP is to look at the strain history of overlap length (the black line in Figure 7a) as it is shown in Figure 7c. In this figure, each curve is the strain along the overlap (black line) at a certain time or load. As indicated by a circle, many curves are passing a common point with the zero value of strain located at 17.4 mm. These curves represent the strain distributions on the overlap length when the joint is still undamaged. When the damage starts propagating in the joint, the curves do not cross the ZSP (black circle point) anymore. It is observed that the DIC was not able to record the displacement and strains very close to the edges of the joint, especially the unloaded edge of the bonding area. This is because when the specimen moves or rotates, and the damage grows, the light and the focus worsen, losing resolution. Subsequently, a rise in the strain history (red oval in Figure 7c) might be observed at the joint edge, especially at the unloaded edge.

Figure 7d demonstrates the ZSP behavior with respect to the load-displacement curve of the SLJ, illustrating how the strain changes in this point as the load increases. As can be seen, as long as the load-displacement curve is in the elastic zone the strain in the ZSP is approximately zero. As the damage starts growing and the load-displacement curve exits the elastic zone the ZSP records negative strains up to the joint failure. In other words, ZSP is the point where strain is initially approximately zero and remains unchanged until the damage starts propagating in the joint, after which the strain in ZSP increases negatively up to the point of joint failure. The ZSP for a joint could be found experimentally using DIC and Fiber Optic Sensors. DIC could serve as a preliminary analysis to design an in-situ analysis that uses Fiber Optic Sensors or strain gauges to monitor the health conditions of the joint.

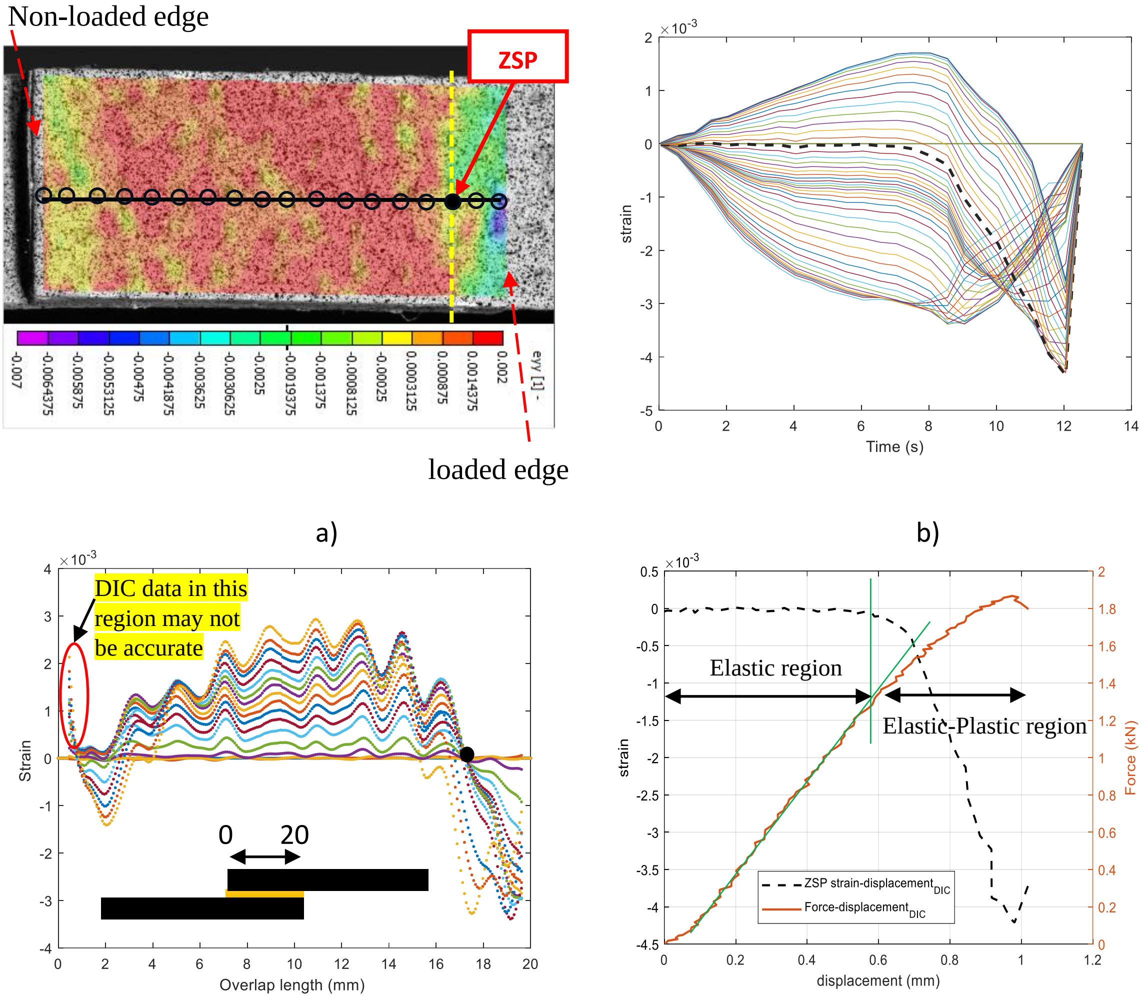

a)

b)

c)

d)

Figure 7 Zero strain point (ZSP) behavior in a joint, e.g., L2W1T1. a) Strain map on the joint area backface b) Strain history of different points on the joint backface (the black dashed line is the strain history of ZSP) c) Strain history of the overlap length on the averaged line (black line) d) Concordance between the ZSP strain curve and joint Force-displacement

3.3. Validation of the ZSP using optical fiber sensors

In Section 3.2, the DIC analysis illustrated that the ZSP is trustworthy enough to predict the behavior of a joint. However, this methodology using DIC cannot be used as an in-situ methodology. For this reason, optical fibers have been adopted and studied to assess whether they can lead to reliable results. Samples L2W2T2 and L2W2T3 were equipped with fibers, on both sides of the overlap area, as reported in Section 2.1. Figure 8a, and b show, respectively, the strain signals recorded by fibers installed on the backfaces (two on each face) of samples L2W2T2 and L2W2T3. For a better visualization only two fibers are shown in Figure 8a,b. The maximum positive and negative strains are different for each sample. L2W2T2 experienced a maximum positive and negative strain of $1.5e^{-3}$, and $-5e^{-3}$, respectively. In case of sample L2W2T3, these values are $8e^{-5}$, and $-3.3e^{-3}$, respectively. Therefore, by increasing the substrate thickness from T2 to T3 the absolute value of positive and negative strain reduces by 95% and 34%, respectively. Since the results of each fiber were approximately the same (Figure 8a,b) as the others, only one of them (Figure 8c,d) is chosen and explained. For example, for specimen L2W2T2, Figure 7a, the first signal and for L2W2T3 (Figure 7b) the second signal was chosen. Figure 8a,b show that the specimen with a thicker substrate experienced lower strain and this is due to the higher stiffness that the thicker substrate exhibits. Due to the relatively high acquisition frequency, in Figure 8c,d, one out of each 10 curves was selected for a better visualization and understanding of the data. The ZSP is clearly visible and shown with black circles. This analysis carried out with the optical fibers led to the same outcomes found with DIC analysis, reported in section 3.2, on the ZSP. Finally, Figure 8e,f show both the evolution of the strain in ZSP from optical fibers and DIC vs. crosshead displacement matching different stages of the specimen force-displacement curve. As can be seen, very similar results were obtained by comparing the strains measured by optical fibers and DIC methodology. Another point to be noticed is that the rise in the unloaded edge is not visible here in optical fiber sensors curves. This is as a result of the Fiber Optic Sensors that can measure the strain also at the joint ends proximity if they are well bonded on the surface.

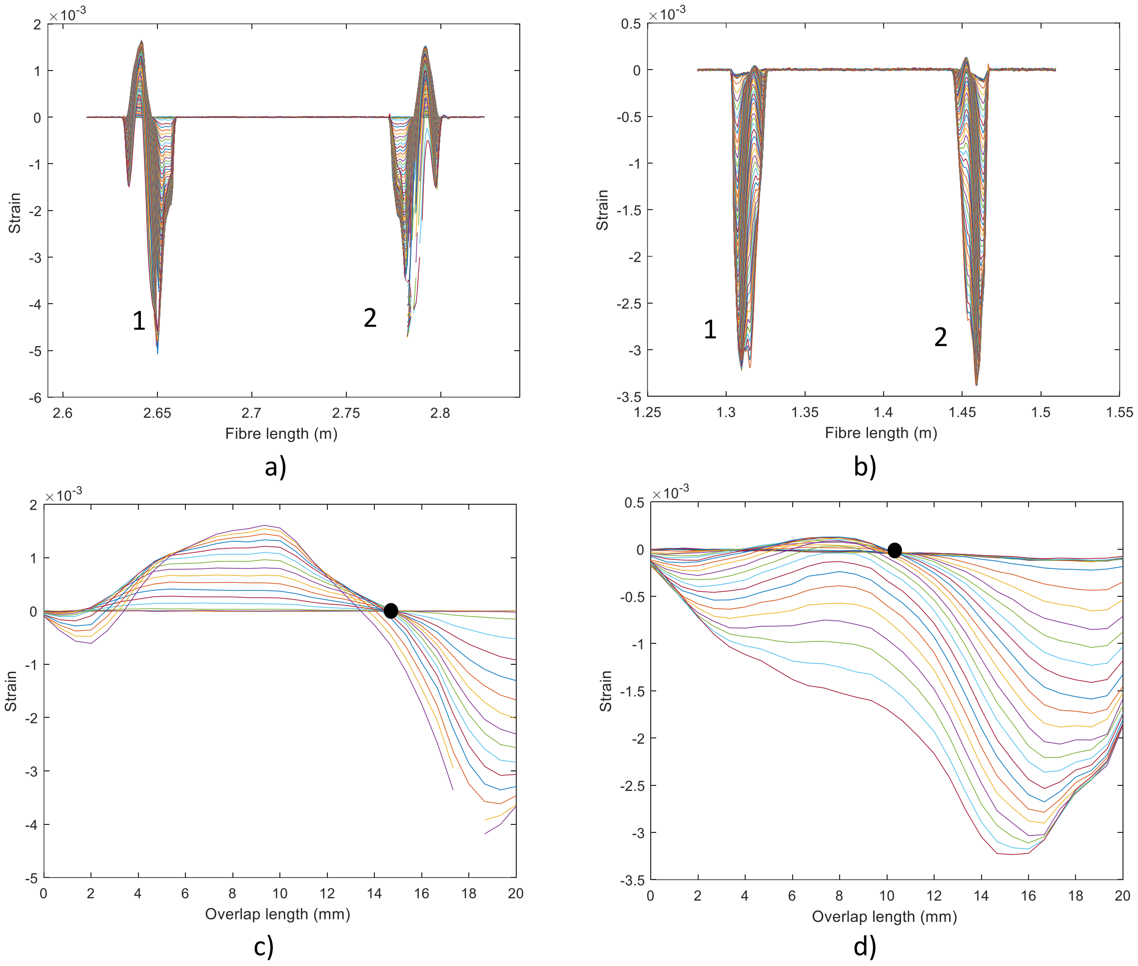

a)

b)

c)

d)

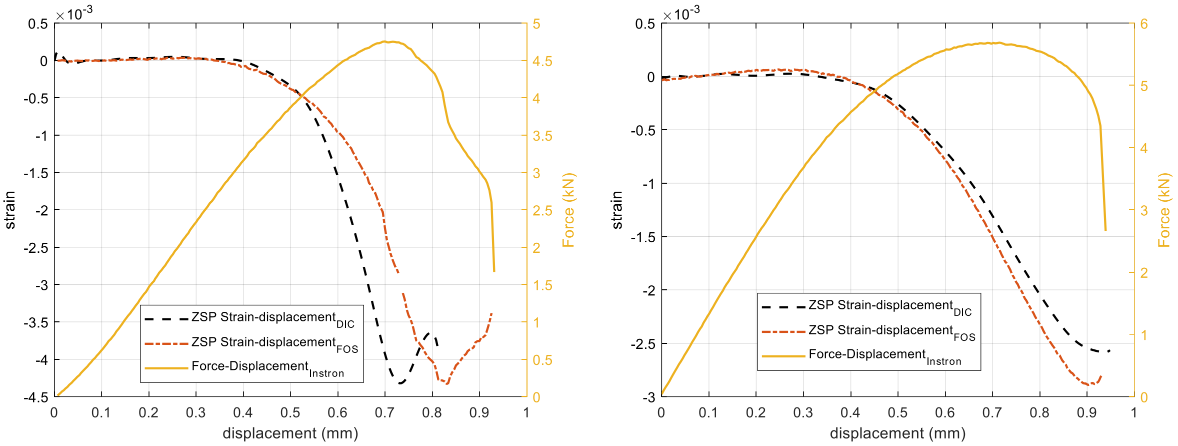

e) f)

Figure 8 ZSP for specimen L2W2T2 and L2W2T3 using both FOS (LUNA) and DIC a) FOS (LUNA) signals for L2W2T2 b) FOS (LUNA) signals for L2W2T3 c) 1st signal is selected and filtered for L2W2T2 d) 2nd signal is selected and filtered for L2W2T3 e) ZSP strain and force-displacement of L2W2T2 f) ZSP strain and force-displacement of L2W2T3

3.4. Damage progression in the joint

Monitoring the backface strain with both DIC and optical fiber sensors provides also more information about how the damage propagates inside the joint. Figure 9a,b,c,d,e,f,g,h and i show the progressive damage of the specimen as well as the change of the strain in ZSP during the test. The strain contour is chosen and fixed based on the strain range in the ZSP so that it remains the same during the test. The dashed yellow line represents the ZSP on the overlap length. As can be seen at the primary stage of loading, Figures 8a, b, c, d and e, the ZSP starts appearing on the surface of the substrate near the non-free edge of the bonding area. The contour color remains the same up to damage initiation (Figure 9f). Then the damage starts propagating in the bonding area from both ends of the joint. The damage propagation from both ends is accompanied by recording the negative strain. However, the quantity of the negative strain is larger on the non-free end of the joint where the ZSP is formed. The results of the DIC on the free end of the joint might not be very precise due to some noise sources, (e.g., light and focus) and that is why in some strain history graphs at the end of the joint a sharp increase in the strain might be seen. However, the result that the damage propagates from both ends but mainly from the loaded end is also supported by the optical fiber sensor which does not present the DIC problems since it is properly bonded on the surface during the test. In Figure 8c,d it is observed that the negative strain is present on both ends of the joint because the quantity of the negative strain on the loaded end is much larger. Figure 9g, h, and i illustrate how the strains in the ZSP become negative due to the damage propagation.

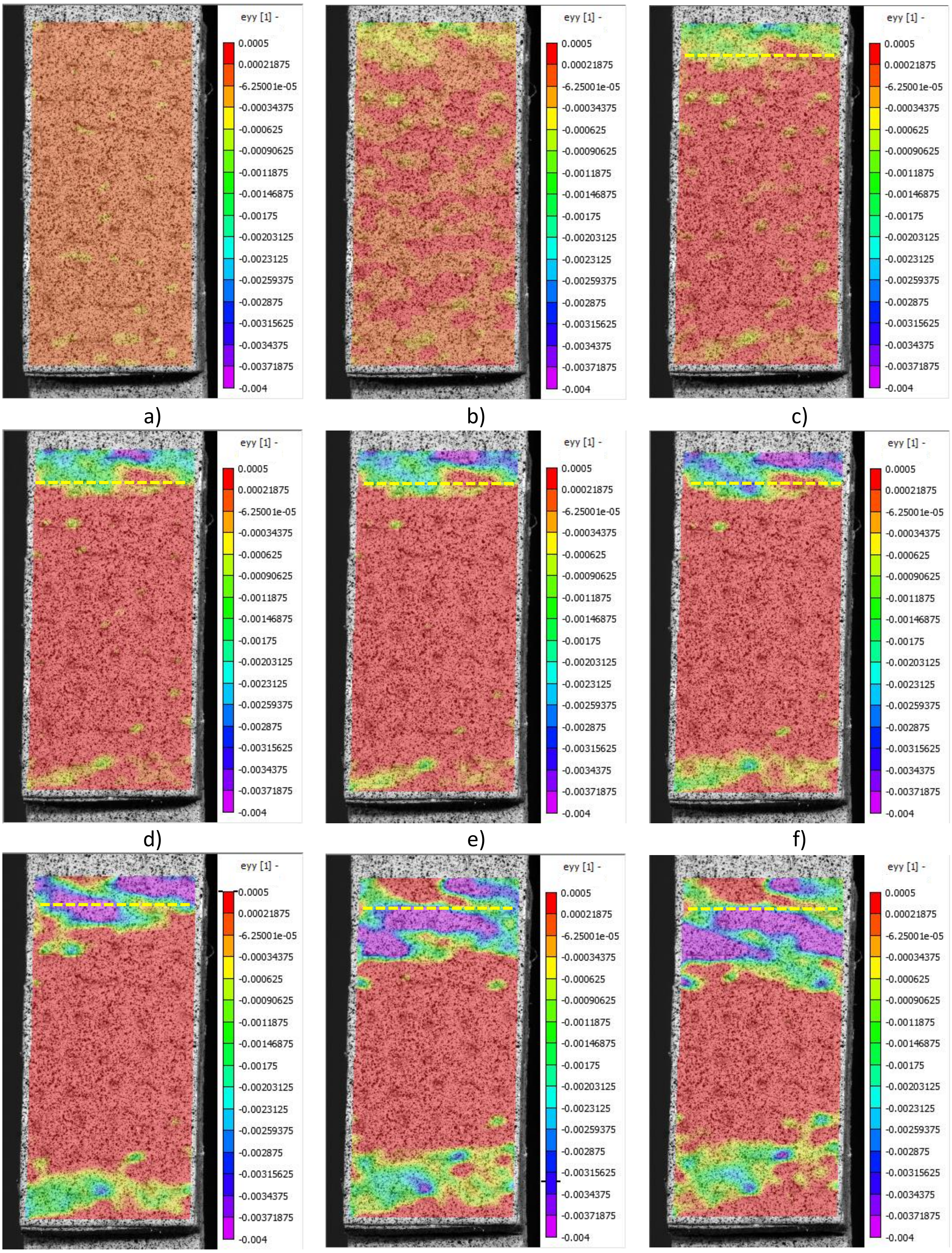

a) b) c) d) e) f) g) h) i)

Figure 9 Damage progression in the joint L2W2T1 a) clamped specimen (Initial condition) b) primary stage of loading (70N) c) elastic zone: the ZSP appears (193 N) d) elastic zone (562.1N) e) elastic zone (1000N) close to damage initiation f) ZSP gains strain: Damage initiated (1380N) g) Damage progression (1653 N) h) Damage progression (1867 N) i) Damage progression up to the rupture (1796N)

3.5. Effect of bonding area geometry on the position of ZSP using DIC

Having the ZSP introduced and verified, the question of this section is: does the bonding area geometry change the location of the ZSP? To answer this question, as already anticipated in section 2.1, a design of experiment has been conducted which considers the overlap length (L), joint width (W) and substrate thickness (T). After the tests have been done and monitored with the DIC the results are explained as follows.

Figure 10a, b, c, d, e and f show the strain distribution on the overlap length for all the specimens (same as explained in section 3.2) with substrate thickness T1. In particular, Figure 10a, c and e (left part of Figure 10) report the strains along the overlap at fixed L1 and T1 and for W1, W2 and W3 respectively. Figure 10b, d and f (right part of Figure 9) report the strains along the overlap area for SLJ prepared with L2, T1 and the three different widths W1, W2 and W3. This analysis shows that considering a fixed overlap length and substrate thickness, the position of ZSP remains approximately unchanged by increasing the joint width. For specimens with T1, ZSP is located at 7.3±0.4 mm and 16.8±0.5 mm respectively for the overlap length of L1 and L2. This implies that the effect of the joint width is negligible on the position of the ZSP. This is probably due to the lack of influence of the joint width on the response of SLJs [41,42]. Considering the joint width and substrate thickness, it can be concluded that the position of the ZSP moves toward the bonding area edge which is loaded as the overlap length is increased.

As the effect of W has proven to be negligible, for the substrate thicknesses T2 and T3 only W2 has been considered for further analyses. Figure 11a, c (left part of Figure 11) show the result for the specimens with substrate thickness T2, and Figure 11b, d (right part of Figure 11) show the result for the specimens with substrate thickness T3. For the specimen with a substrate thickness of T2, the ZSP is located at 5.3±0.2 mm and 14.2±0.2 mm, respectively, when the overlap length is L1 and L2. For the specimen with a substrate thickness of T3, the ZSP is located at 3.5±1 mm and 10±0.2 mm, respectively, when the overlap length is L1 and L2. As illustrated in the analysis reported in Figure 10 and Figure 11, by increasing the substrate thickness, the strains on the overlap length tend to be closer to zero or negative. This is because thicker and stiffer substrates experience less strain, which can be observed by comparing L1W2T1 (Figure 10c), L1W2T2 (Figure 11a), and L1W2T3 (Figure 11b). Additionally, increasing the substrate thickness causes the ZSP to shift toward the center of the joint or to the other zone of the joint near the free end of the bonding area (Figure 12). This can be ascribed to the prevailing negative strain caused by the bending moment with respect to the positive strain caused by tension when the substrate is thicker. Finally, by comparing the results for specimens with different substrate thicknesses (Figure 10 and Figure 11) it is illustrated that as the substrate thickness increases the positive strain values on the overlap length becomes smaller. This is because the thinner substrates undergo deformation more easily than they can be recorded by strain measuring tools. This implies that the backface strain method is more reliable and evident in specimens with thinner substrates.

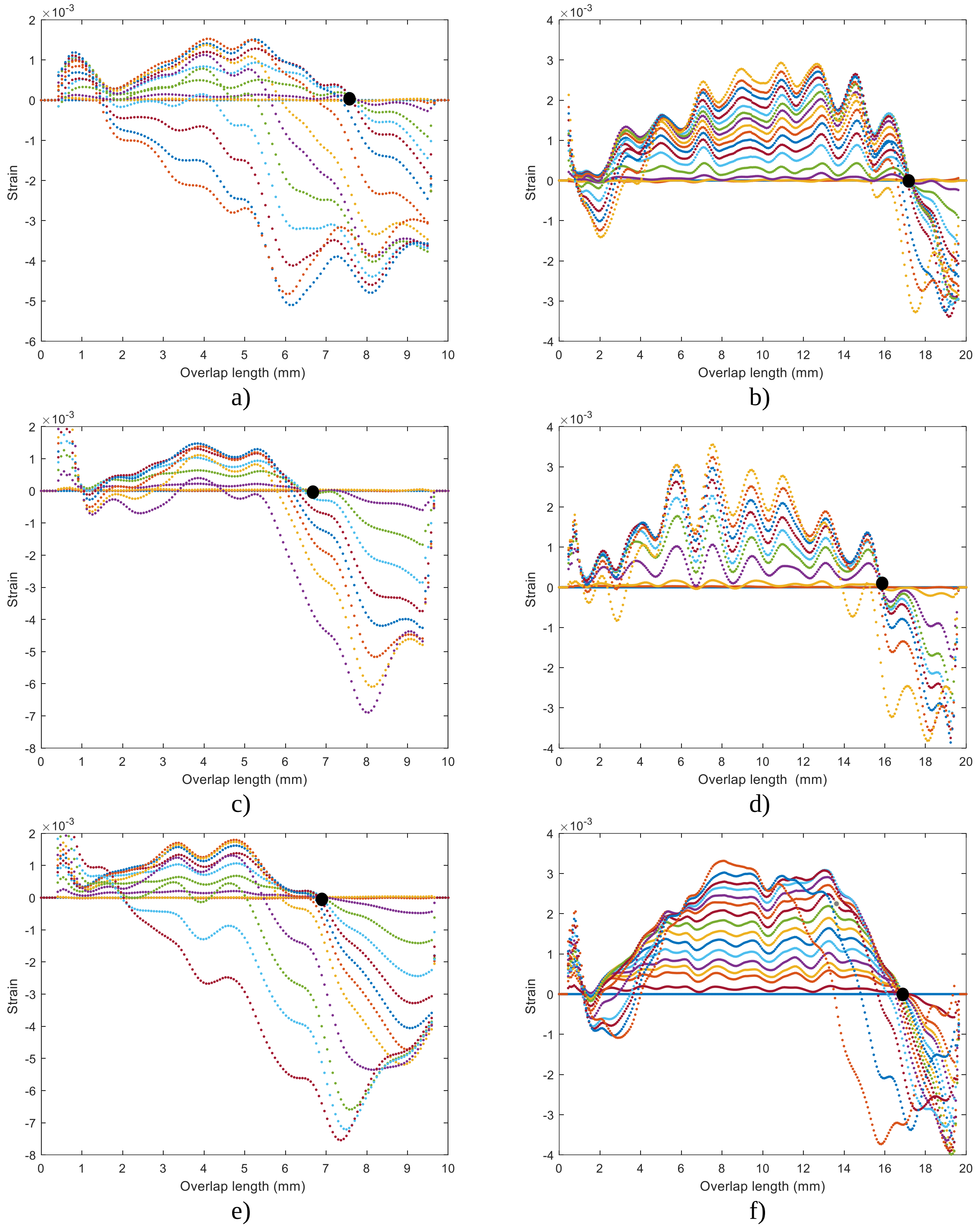

a) b)

c) d)

e) f)

Figure 10 effect of bonding area dimension on the position of ZSP for substrate T1 a) L1W1T1 b) L2W1T1 c) L1W2T1 d) L2W2T1 e) L1W3T1 f) L2W3T1

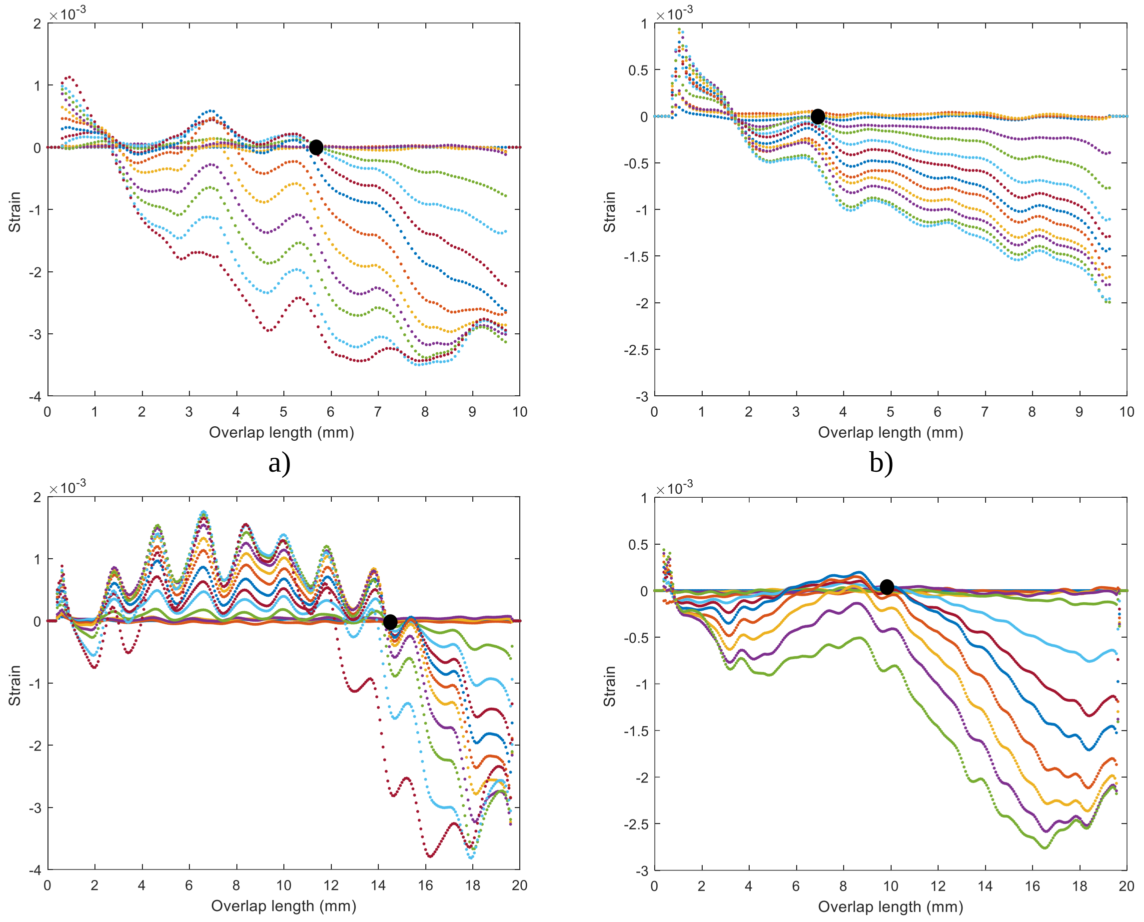

a)

b)

c)

d)

Figure 11 ZSP position for specimen with substrate thickness of T2 and T3 a) L1W2T2, b) L1W2T3, c) L2W2T2, d) L2W2T3

To summarize the effect of joint area dimension on the position of ZSP, Figure 12 provides an overview of the results for all the joints together. The joint overlap length is normalized in order to include also the effect of overlap length in one figure. In general, the substrate thickness played the most important role in the position of the ZSP. The second important parameter is the overlap length, and finally, the joint width showed the least importance. That is why a generic letter W is used in Figure 12.

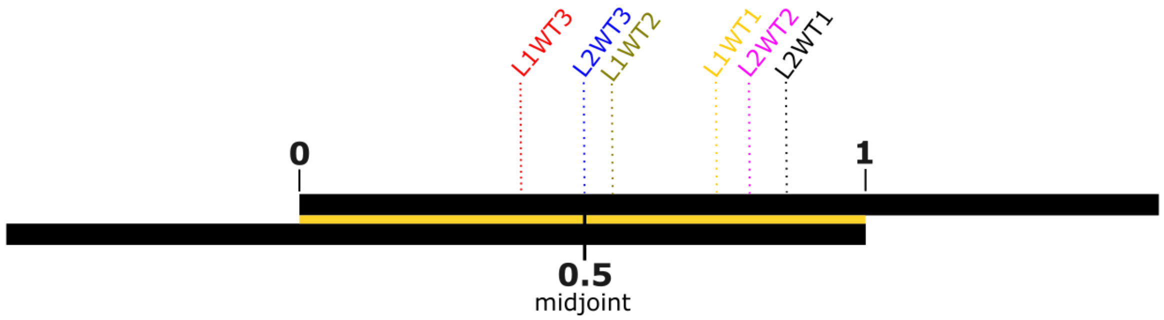

Figure 12 Summarizing the effect of joint dimensions on the position of ZSP (normalized overlap length)

Another point that is worth mentioning is that the strain map for composite substrates looks wavy (for example, Figure 7c) when the DIC is used to acquire the strain due to the intrinsic texture of composite materials. A microscopic image of the composite substrate is shown in Figure 13a. It is mentioned in section 3.2 that each nominated point on the overlap length (Figure 7a) is the average of all the points on the joint width with the same position on the overlap length. For example, the orange point (Figure 13a) is the average of the strain on the orange line and the blue point is the average of the blue line. Each line includes both warp and weft but not with the same ratio. This concept is emphasized in Figure 13b. As can be seen, the blue line can contain more resin, more warp with E_{fl} (longitudinal modulus) and less weft with E_{ft} Young modulus. Whilst, the orange line contains less resin, less warp with E_{fl} (transversal modulus) and more weft with E_{ft} Young modulus. Usually, the modulus of the yarn in the longitudinal direction is higher compared to its modulus in the transversal direction ($E_{ft} < E_{fl}$). Therefore, the peaks can be related to the sections (the orange line which contains more of E_{ft}) with a smaller resultant Young modulus because based on the Hooke law those parts undergo larger strain. Based on the same approach, valleys can be due to the sections (the blue line which contains more of E_{fl}) with larger resultant Young modulus.

On the other hand, the strain history obtained from the optical fibers (Figure 8c,d) is smooth in comparison with the ones obtained by DIC. The reason is related to the high resolution of the DIC analysis. On the other hand, the optical fiber sensors use a gauge pitch as a measuring point (Section 2) of 0.65 mm which does not allow to detect the peaks and valleys in the analyzed area. Furthermore, as the backface strain for specimens L2W2T2 and L2W2T3 were also measured by the optical fibers it is possible to compare the optical strain history of these two samples with the ones of DIC. Comparing Figure 8c with Figure 11c and Figure 8d with Figure 11d, it is evident that both strain measuring devices indicate the same point at the ZSP on the overlap length. The only difference is that the optical fibers record more precise data at the edges as explained in Sections 3.2 and 3.3.

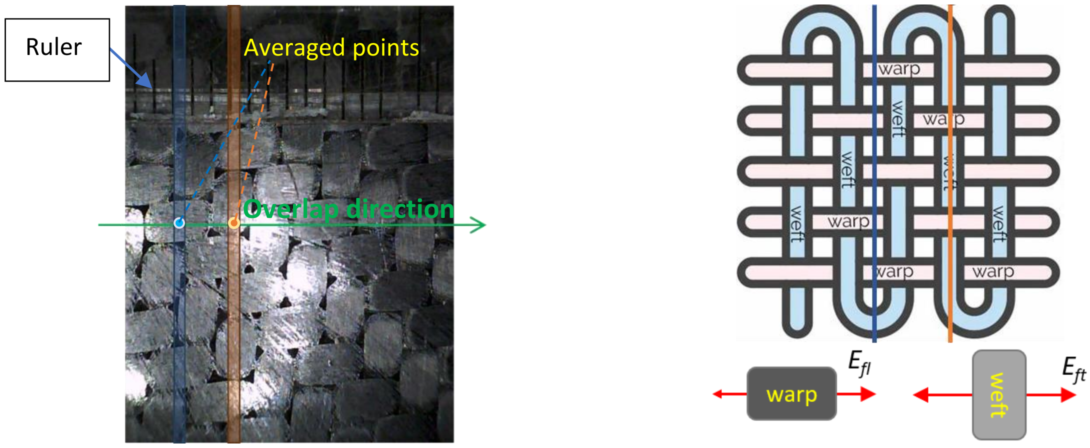

a) b)

Figure 13 Composite substrate texture a) microscopic image of the laminate b) Ideal schematic of the laminate texture

4. Cyclic loading

The results presented in Section 3 demonstrated that the ZSP method can be detected with both DIC and optical fibers. Further, these methods can monitor the damage initiation and propagation in SLJs with different bonding area dimensions under normal tensile loading. However, structures and adhesive bonding joints could practically be subjected to cyclic or fatigue loads. In this section, the effect of cyclic loading on damage initiation and propagation of an SLJ using both DIC and optical fiber is studied. The ZSP method is employed as the criteria for the prediction of joint behavior.

Sample L2W1T2 (L=20 mm, W=10 mm, and T=20 mm) was used to study how the strain in the ZSP varies under cyclic loading and whether the strain in ZSP changes from zero when plastic deformation is accumulated in the joint. A six-cycle loading was considered in a way that in each cycle the load increases at a constant velocity of 5 mm/min up to a certain amount, and then unloading starts with the same velocity up to 50 N. After that, the next cycle starts considering the same velocity for loading and unloading. The maximum load for the first, second, third, fourth, fifth and sixth cycles are, respectively, 1 kN, 1.5 kN, 2 kN, 2.2 kN, 2.4 kN, and up to the sample rupture (for this sample happened at approximately 2 kN). Figure 14 shows the load-displacement curve for sample L2W1T2 subjected to the mentioned cyclic loading. As can be seen in Figure *14*, after the first and second cycle the joint is still undamaged, and the unloading curve is following the loading curve. The quite small variation in the displacement is due to the initial clearances of the joint. In the third cycle, the peak load falls on a line which passes the first and second cycles' peaks. This could be interpreted as the healthiness of the joint up to the third cycle peak load. However, there is a difference (approximately 28%) between the third unloading curve and the first loading curve, which signals the damage initiation. After the third cycle, the cycles' peaks are not in a line anymore which again indicates that the damage has already been initiated. Moreover, the difference between the fourth unloading curve and the first loafing curve becomes even larger (approximately 70%). In the fifth cycle, this difference is 150% and the crack grows noticeably in the joint. Finally, the sixth cycle is where the crack grows up to the joint rupture.

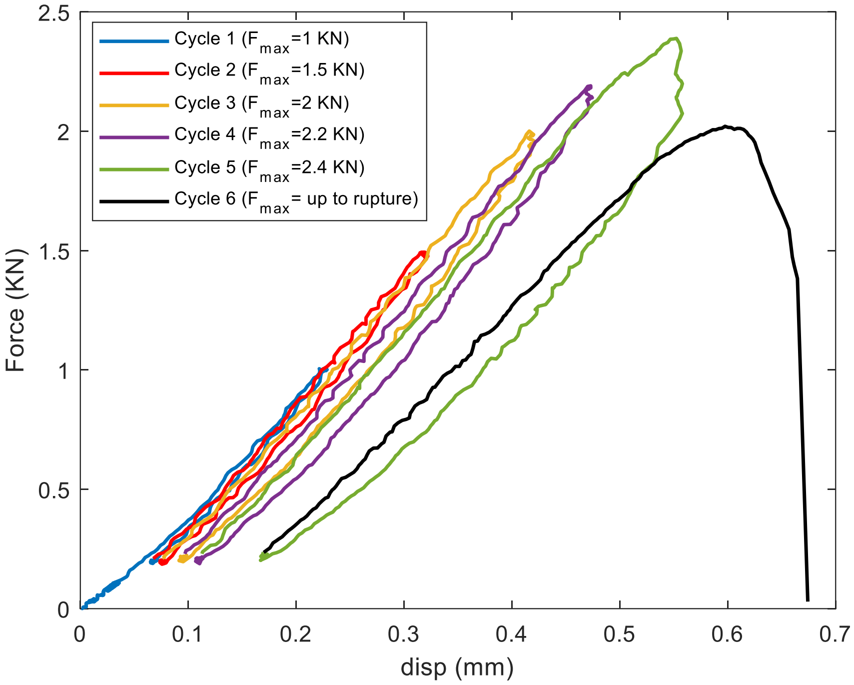

Figure 14 Load displacement curve for sample L2W1T2 under cyclic loading

Having the loading cycles explained, Figure 15a, b, c, d, e and f illustrate the strain on the backface of L2W1T2 overlap length at each complete cycle. The solid lines are representatives of the data from optical fibers, and the dashed lines represent the data from DIC. As can be seen in Figures 14, the maximum recorded strains by the optical fiber are larger than the maximum strain recorded by the DIC. This is because of the texture of the composite materials and the fact explained in detail in section 3.5 about the waviness of DIC strain histories on the overlap length. For the same reason, looking at the strain curves from the DIC data, a sort of plateau is visualized in the mid-area of the joint.

According to the results of Figure 14, after the first and second cycle the joint is still in a healthy condition, and this could be verified by results provided in Figure 15a,b. Figures a and b show that the ZSP has still a value of zero strain after the first and second cycles. In the third cycle (Figure 15c) the damage initiates as the ZSP starts recording a small negative value. However, before the crack starts propagating the unloading starts. The ZSP is located initially at 15 mm (shown with a black circle) and remains at the same position until the end of the 3rd cycle. In the 4th cycle, ZSP is shown with the purple circle. It can be seen that the ZSP is slightly shifted to the left close to 14 mm, i.e., the crack propagated but to a small extent and again unloading starts. After the crack stopped propagating in the unloading part, a new point (blue circle) appears on the graph (Figure 15d) with a negative constant value (close to zero) over time. The position of this point is where the ZSP will appear in the next cycle. This is because the effective overlap length of the joint decreases after each cycle in such a way that after each cycle it can be assumed that the loading is being applied to a joint with a shorter overlap length. This new point appears in the unloading part of the cycle and exactly when the crack stops propagating. As the unloading part of each cycle is close to the loading part of the next cycle (Figure 14), this point represents the ZSP for the next cycle. In 5th cycle (Figure 15e), the blue circle defines the ZSP which is at the same position predicted in the 4th cycle. Here, the crack propagates to a large extent, but the joint has not yet reached the rupture. Therefore, the position of the new ZSP will be estimated in the unloading part as the empty red circle. Finally, in the 6th cycle (Figure 15f), the crack propagates completely, and the substrates are detached.

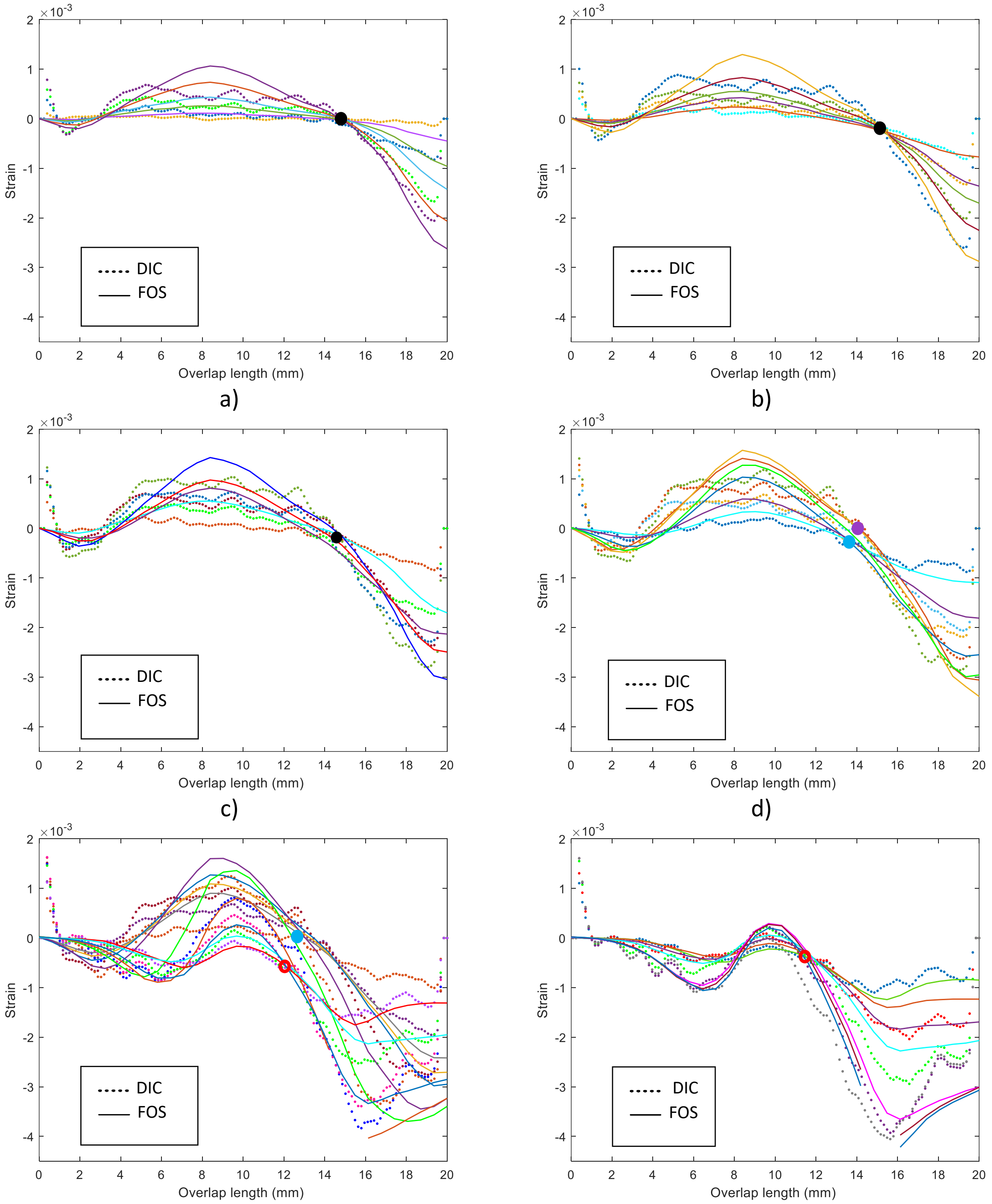

a)

b)

c)

d)

e) f)

Figure 15 Backfce strain distribution at each cycle up to the rupture for specimen L2W1T2 a) cycle 1(F_{max} = 1 kN): healthy condition b) cycle 2 (F_{max} = 1.5 kN): healthy condition c) cycle 3(F_{max} = 2 kN): damage initiation d) cycle 4 (F_{max} = 2.2 kN): small damage propagation e) cycle 5 (F_{max} = 2.4 kN): noticeable damage propagation f) cycle 6 (F_{max} = 2 kN): damage propagation up to rupture

In cyclic loading, there are two ways to analyze the joint. The first one is that at each cycle it can be assumed that the loading is being applied to a new SLJ with its own ZSP. It is enough to monitor the related ZSP strain at each cycle and understand the behavior of the joint as it is done for a normal SLJ subjected to tensile loading. As in real components, it might not be possible to install the DIC because of its dimensions, and as explained before the effective overlap length of the joint changes in each cycle it might not be precise to use strain gauges. Therefore, to use this approach optical fibers are the most useful tool to be employed by monitoring the initial ZSP continuously. Figure *16*a shows the strain history versus time for points on the overlap length the same as already explained in section 3.2 for Figure *7*b. Solid lines show DIC data while dashed lines present optical fiber data. In Figure *16*a, different cycles can be easily distinguished. In general, when the strain increases in absolute value it means the sample is in the loading phase of the cycle otherwise the sample is in the unloading phase. Therefore, after each absolute minimum value of strain, the next cycle is going to start. As expected, there are not too many points with a strain value of zero when the joint is still in healthy condition. Those points are representative of the ZSP which correspondence to the black circles in Figure *15*a, b and c. By plotting the strain history of the original ZSP vs time as well as Force vs time in the same graph (Figure *16*b) the performance of ZSP and the behavior of the joint can be explained better. As explained previously in this section based on Figure *14* and Figure *15*, and according to Figure *16*b, the joint is in a safe condition up to the peak of the third cycle because the ZSP strain remains approximately around zero. In the unloading phase of 3rd cycle, a small drop can be seen in the ZSP strain curve. This might signal the damage initiation, but it is not yet confirmed because ZSP might go back to zero value at the end of the unloading phase. Since the curves are being filtered there is a possibility to find a point very close to the real ZSP instead of the real ZSP itself. This will result in an oscillation close to zero in the found ZSP value. In the 4th cycle, the ZSP starts gaining value before reaching zero value. This confirms that the damage was initiated in the previous cycle. Up to the 4th cycle, the crack starts propagating by the force reaching its maximum value and in the unloading phase. In the 5th cycle, the propagation starts shortly before the peak load, and in the loading phase with a drastic drop in the ZSP value at peak load. Finally, in the 6th cycle, the crack starts propagating shortly after the loading started and the joint arrives at the rupture at peak force.

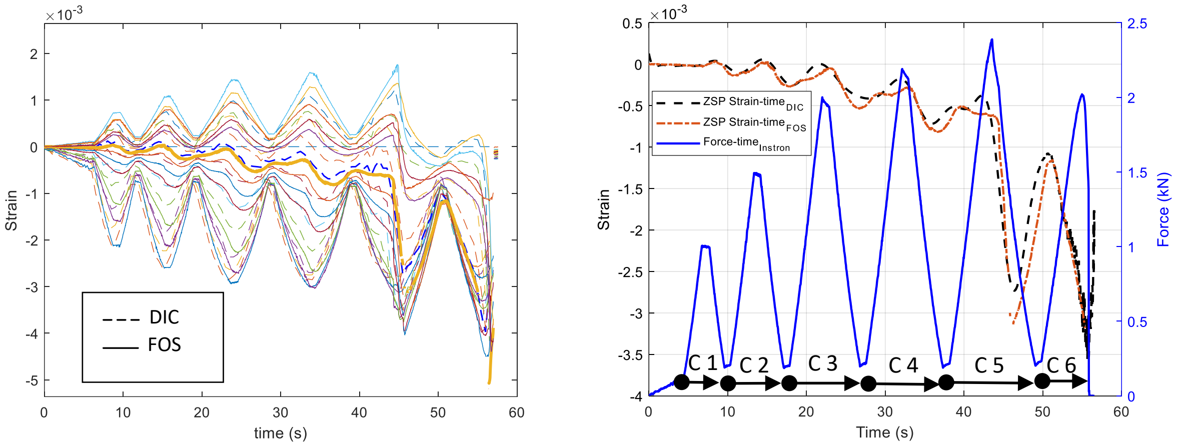

a) b)

Figure 16 ZSP strain using DIC and FOS (LUNA) as well as L2W1T2 force diagram versus the time

5. Conclusion

The present work aims to propose the so-called zero strain point (ZSP) as a criterion to monitor the health condition of composite single lap joints. Furthermore, the effectiveness and reliability of this method were studied when the joint dimension (in particular, adherend thickness, joint width, overlap length), and loading type (quasi-static and cyclic) change. To validate the results tests were performed with DIC (digital image correlation) system and Fiber Optic Sensors. The drawn conclusions are as follows:

- Considering both cyclic and static tensile loading conditions, the ZSP point can be utilized as a criterion for adhesive SLJs to predict the damage initiation and propagation up to the rupture. This fact was verified precisely with both DIC and optical fiber results.
- According to the optical fiber results, both sides of SLJs (both loaded and fixed adherends) experience approximately the same strain. Therefore, to the ZSP method, it is enough to observe the strain on the backface of one adherend.
- Based on the DIC backface strain map, the damage initiates and propagates from both ends of the bonding area taking into account that the propagation is slightly faster from the loading side of the joint.
- The joint width showed negligible effect on the position of ZSP in joints with both adhesive types.
- In joints with larger overlap lengths, the passage from positive to negative strain allows for better detection of the ZSP position. Therefore, the ZSP is more reliable in joints with larger overlap lengths.
- Increasing the substrate thickness causes the ZSP to move toward the middle or free edge of the joints. the same results were obtained by decreasing the overlap length.
- When the substrate thickness is relatively large, and the overlap length is relatively short, only negative strains are observed in joints. Therefore, the ZSP might not be clearly visible, and this implies a limitation on the application of the ZSP.
- The strain history on the SLJs’ overlap length is wavy when analyzing the DIC data due to the texture of composite materials. Conversely, it is smooth when the FOS (LUNA) data is being considered because the strain will be recorded based on the optical fiber deformations.
- In cyclic loading, although each cycle has its own ZSP which can be used as the criterion to observe the joint condition after the damage initiation, it would be easier and more effective to use the primary ZSP before the damage initiation to monitor the joint behavior.
- Although DIC might not be installed on a component to monitor the healthy condition of the joint, optical fibers could be mounted in order to do an online and in-situ monitoring of the joints.

Declaration of AI and AI-assisted technologies in the writing process:

During the preparation of this work, the author(s) used ChatGPT 4 and Quillbot to improve the text's grammar. After using this tool/service, the author(s) reviewed and edited the content as needed and take(s) full responsibility for the publication's content.

Funding: The research work was carried out in a PhD program partially funded with a scholarship by J-Tech@PoliTO-Advanced Joining Technologies.

References

[1] Budhe S, Banea MD, de Barros S, da Silva LFM. An updated review of adhesively bonded joints in composite materials. Int J Adhes Adhes 2017;72:30–42. https://doi.org/10.1016/J.IJADHADH.2016.10.010.

[2] Zhang J, Lin G, Vaidya U, Wang H. Past, present and future prospective of global carbon fibre composite developments and applications. Compos B Eng 2023;250:110463. https://doi.org/10.1016/J.COMPOSITESB.2022.110463.

[3] Li W, Palardy G. Damage monitoring methods for fiber-reinforced polymer joints: A review. Compos Struct 2022;299:116043. https://doi.org/10.1016/J.COMPSTRUCT.2022.116043.

[4] Wei Y, Jin X, Luo Q, Li Q, Sun G. Adhesively bonded joints – A review on design, manufacturing, experiments, modeling and challenges. Compos B Eng 2024;276:111225. https://doi.org/10.1016/J.COMPOSITESB.2024.111225.

[5] Jeevi G, Nayak SK, Abdul Kader M. Review on adhesive joints and their application in hybrid composite structures. J Adhes Sci Technol 2019;33:1497–520. https://doi.org/10.1080/01694243.2018.1543528.

[6] Gerhard T, Friedrich C. Mechanical fastening of carbon composite tubes, numerical calculation of axial loading capacity and experimental verification. Compos B Eng 2014;67:391–9. https://doi.org/10.1016/J.COMPOSITESB.2014.07.024.

[7] Jung I, Kim J, Kim E, Kim CD, Kim NR, Yang CM, et al. Enhanced composite laminate fastening and delamination repair using hierarchical thermoplastic composite rivets. Compos B Eng 2024;277:111382. https://doi.org/10.1016/J.COMPOSITESB.2024.111382.

[8] Ramalho LDC, Campilho RDSG, Belinha J, da Silva LFM. Static strength prediction of adhesive joints: A review. Int J Adhes Adhes 2020;96:102451. https://doi.org/10.1016/J.IJADHADH.2019.102451.

[9] Tserpes K, Barroso-Caro A, Carraro PA, Beber VC, Floros I, Gamon W, et al. A review on failure theories and simulation models for adhesive joints. J Adhes 2022;98:1855–915. https://doi.org/10.1080/00218464.2021.1941903.

[10] Shang X, Marques EAS, Machado JJM, Carbas RJC, Jiang D, da Silva LFM. Review on techniques to improve the strength of adhesive joints with composite adherends. Compos B Eng 2019;177:107363. https://doi.org/10.1016/J.COMPOSITESB.2019.107363.

[11] Weiland J, Sadeghi MZ, Thomalla J V., Schiebahn A, Schroeder KU, Reisgen U. Analysis of back-face strain measurement for adhesively bonded single lap joints using strain gauge, Digital Image Correlation and finite element method. Int J Adhes Adhes 2020;97:102491. https://doi.org/10.1016/J.IJADHADH.2019.102491.

[12] Crocombe AD, Ong CY, Chan CM, Abdel Wahab MM, Ashcroft IA. Investigating fatigue damage evolution in adhesively bonded structures using backface strain measurement. Journal of Adhesion 2002;78:745 – 776. https://doi.org/10.1080/00218460213835.

[13] Zhang Z, Shang JK, Lawrence F V. A Backface Strain Technique for Detecting Fatigue Crack Initiation in Adhesive Joints. J Adhes 1995;49:23–36. https://doi.org/10.1080/00218469508009975.

[14] Sánchez-Romate XF, Sbarufatti C, Sánchez M, Bernasconi A, Scaccabarozzi D, Libonati F, et al. Fatigue crack growth identification in bonded joints by using carbon nanotube doped adhesive films. Smart Mater Struct 2020;29:035032. https://doi.org/10.1088/1361-665X/ab7109.

[15] Augustin T, Karsten J, Kötter B, Fiedler B. Health monitoring of scarfed CFRP joints under cyclic loading via electrical resistance measurements using carbon nanotube modified adhesive films. Compos Part A Appl Sci Manuf 2018;105:150–5. https://doi.org/10.1016/j.compositesa.2017.11.015.

[16] Kang MH, Choi JH, Kweon JH. Fatigue life evaluation and crack detection of the adhesive joint with carbon nanotubes. Compos Struct 2014;108:417–22. https://doi.org/10.1016/J.COMPSTRUCT.2013.09.046.

[17] Roth W, Giurgiutiu V. Structural health monitoring of an adhesive disbond through electromechanical impedance spectroscopy. Int J Adhes Adhes 2017;73:109–17. https://doi.org/10.1016/J.IJADHADH.2016.11.008.

[18] Zhuang Y, Kopsaftopoulos F, Dugnani R, Chang F-K. Integrity monitoring of adhesively bonded joints via an electromechanical impedance-based approach. Struct Health Monit 2018;17:1031–45. https://doi.org/10.1177/1475921717732331.

[19] Bak KM, KalaiChelvan K, Vijayaraghavan G, Sridhar B. Acoustic emission wavelet transform on adhesively bonded single-lap joints of composite laminate during tensile test. Journal of Reinforced Plastics and Composites 2013;32:87–95. https://doi.org/10.1177/0731684412459249.

[20] Saeedifar M, Saleh MN, De Freitas ST, Zarouchas D. Damage characterization of adhesively-bonded Bi-material joints using acoustic emission. Compos B Eng 2019;176:107356. https://doi.org/10.1016/J.COMPOSITESB.2019.107356.

[21] Koecher MC, Pande JH, Merkley S, Henderson S, Fullwood DT, Bowden AE. Piezoresistive in-situ strain sensing of composite laminate structures. Compos B Eng 2015;69:534–41. https://doi.org/10.1016/J.COMPOSITESB.2014.09.029.

[22] Gackowski BM, Goh GD, Sharma M, Idapalapati S. Additive manufacturing of nylon composites with embedded multi-material piezoresistive strain sensors for structural health monitoring. Compos B Eng 2023;261:110796. https://doi.org/10.1016/J.COMPOSITESB.2023.110796.

[23] Vijaya Kumar RL, Bhat MR, Murthy CRL. Evaluation of kissing bond in composite adhesive lap joints using digital image correlation: Preliminary studies. Int J Adhes Adhes 2013;42:60–8. https://doi.org/10.1016/J.IJADHADH.2013.01.004.

[24] Comer AJ, Katnam KB, Stanley WF, Young TM. Characterising the behaviour of composite single lap bonded joints using digital image correlation. Int J Adhes Adhes 2013;40:215–23. https://doi.org/10.1016/J.IJADHADH.2012.08.010.

[25] Li HCH, Herszberg I, Davis CE, Mouritz AP, Galea SC. Health monitoring of marine composite structural joints using fibre optic sensors. Compos Struct 2006;75:321–7. https://doi.org/10.1016/J.COMPSTRUCT.2006.04.054.

[26] Silva-Muñoz RA, Lopez-Anido RA. Structural health monitoring of marine composite structural joints using embedded fiber Bragg grating strain sensors. Compos Struct 2009;89:224–34. https://doi.org/10.1016/J.COMPSTRUCT.2008.07.027.

[27] Zeng H, Yan R, Xu L, Gui S. Application study on fiber Bragg grating sensors in damage monitoring of sandwich composite joints. Journal of Sandwich Structures & Materials 2020;22:1542–63. https://doi.org/10.1177/1099636218789621.

[28] Grundmann N, Brüning H, Tserpes K, Strohbach T, Mayer B. Influence of Embedding Fiber Optical Sensors in CFRP Film Adhesive Joints on Bond Strength. Sensors 2020;20:1665. https://doi.org/10.3390/s20061665.

[29] da Silva LFM, Moreira PMGP, Loureiro ALD. Determination of the strain distribution in adhesive joints using Fiber Bragg Grating (FBG). J Adhes Sci Technol 2014;28:1480–99. https://doi.org/10.1080/01694243.2012.698120.

[30] Janeliukstis R, Chen X. Review of digital image correlation application to large-scale composite structure testing. Compos Struct 2021;271:114143. https://doi.org/10.1016/j.compstruct.2021.114143.

[31] Satoh T, Abe H. Non-Destructive Detection Method of Fatigue Crack in Spot-Welded Joint Specimens. SAE International Congress and Exposition, SAE International; 1986. https://doi.org/https://doi.org/10.4271/860601.

[32] Janetzko-Preisler A, Sadeghi Z, Adomeit A, Schröder K-U. Damage Assessment in Adhesively Bonded Structures by Using SmartSHM. vol. 2. 2015. https://doi.org/10.12783/SHM2015/27.

[33] A. Graner Solana A. D. Crocombe MMAW, Ashcroft IA. Fatigue initiation in adhesively-bonded single-lap joints. J Adhes Sci Technol 2007;21:1343–57. https://doi.org/10.1163/156856107782313629.

[34] Curley AJ, Hadavinia H, Kinloch AJ, Taylor AC. Predicting the service-life of adhesively-bonded joints. Int J Fract 2000;103:41–69. https://doi.org/10.1023/A:1007669219149.

[35] Shenoy V, Ashcroft IA, Critchlow GW, Crocombe AD. Unified methodology for the prediction of the fatigue behaviour of adhesively bonded joints. Int J Fatigue 2010;32:1278–88. https://doi.org/10.1016/J.IJFATIGUE.2010.01.013.

[36] Boursier Niutta C, Tridello A, Ciardiello R, Paolino DS. Strain Measurement with Optic Fibers for Structural Health Monitoring of Woven Composites: Comparison with Strain Gauges and Digital Image Correlation Measurements. Sensors 2023;23:9794. https://doi.org/10.3390/s23249794.

[37] Andrea Bernasconi MK, Comolli L. Strain Profile Measurement for Structural Health Monitoring of Woven Carbon-fiber Reinforced Polymer Composite Bonded joints by Fiber Optic Sensing Using an Optical Backscatter Reflectometer. J Adhes 2016;92:440–58. https://doi.org/10.1080/00218464.2015.1043005.

[38] Sans D, Stutz S, Renart J, Mayugo JA, Botsis J. Crack tip identification with long FBG sensors in mixed-mode delamination. Compos Struct 2012;94:2879–87. https://doi.org/10.1016/J.COMPSTRUCT.2012.03.032.

[39] Bernasconi A, Carboni M, Comolli L. Monitoring of fatigue crack growth in composite adhesively bonded joints using Fiber Bragg Gratings. Procedia Eng 2011;10:207–12. https://doi.org/10.1016/j.proeng.2011.04.037.

[40] Sahin R, Akpinar S. The effects of adherend thickness on the fatigue strength of adhesively bonded single-lap joints. Int J Adhes Adhes 2021;107:102845. https://doi.org/10.1016/j.ijadhadh.2021.102845.

[41] Abbasi M, Ciardiello R, Goglio L. Experimental Study on the Effect of Bonding Area Dimensions on the Mechanical Behavior of Composite Single-Lap Joint with Epoxy and Polyurethane Adhesives. Applied Sciences 2023;13:7683. https://doi.org/10.3390/app13137683.

[42] Abbasi M, Ciardiello R, Goglio L. Effect of bonding area geometry on the behavior of composite single lap joints (SLJ) and estimation of adhesive properties using finite element method. Journal of Adhesion 2023. https://doi.org/10.1080/00218464.2023.2252338.

[43] Reis PNB, Antunes FJV, Ferreira JAM. Influence of superposition length on mechanical resistance of single-lap adhesive joints. Compos Struct 2005;67:125–33. https://doi.org/10.1016/J.COMPSTRUCT.2004.01.018.

[44] Fernández-Cañadas LM, Ivañez I, Sanchez-Saez S, Barbero EJ. Effect of adhesive thickness and overlap on the behavior of composite single-lap joints. Mechanics of Advanced Materials and Structures 2021;28:1111–20. https://doi.org/10.1080/15376494.2019.1639086.

[45] Baykara C. Effects of single-lap joint at different adhesive thicknesses on fatigue strength of metals with different surface coatings. Proc Inst Mech Eng C J Mech Eng Sci 2023:095440622311529. https://doi.org/10.1177/09544062231152995.

[46] Gültekin K, Akpinar S, Özel A. The effect of the adherend width on the strength of adhesively bonded single-lap joint: Experimental and numerical analysis. Compos B Eng 2014;60:736–45. https://doi.org/10.1016/J.COMPOSITESB.2014.01.022.

[47] Djebbar N, Boutabout B, Boulenouar Rachid H, Oudad W. Effect of spew adhesive and beveling substrate geometrical shape on stresses in a bonded single lap joint. Eng Struct 2022;256:114049. https://doi.org/10.1016/j.engstruct.2022.114049.

[48] Ciardiello R, D’Angelo D, Cagna L, Croce A, Paolino DS. Effects of plasma treatments of polypropylene adhesive joints used in the automotive industry. Proc Inst Mech Eng C J Mech Eng Sci 2022;236:6204–18. https://doi.org/10.1177/09544062211065361.

[49] Berntsen JF, Morin D, Clausen AH, Langseth M. Experimental investigation and numerical modelling of the mechanical response of a semi-structural polyurethane adhesive. Int J Adhes Adhes 2019;95:102395. https://doi.org/https://doi.org/10.1016/j.ijadhadh.2019.102395.

[50] Banea MD, da Silva LFM, Campilho RDSG. The Effect of Adhesive Thickness on the Mechanical Behavior of a Structural Polyurethane Adhesive. J Adhes 2015;91:331–46. https://doi.org/10.1080/00218464.2014.903802.

[51] Abbasi M, Alavi Nia A. High-velocity impact behavior of sandwich structures with AL faces and foam cores—Experimental and numerical study. Aerosp Sci Technol 2020;105:106039. https://doi.org/10.1016/J.AST.2020.106039.

[52] Abbasi M, Alavi Nia A, Abolfathi M. Experimental study on the high-velocity impact behavior of sandwich structures with an emphasis on the layering effects of foam core. Journal of Sandwich Structures and Materials 2021;23:3–22. https://doi.org/10.1177/1099636218813412.

[53] Beber VC, Schneider B, Brede M. Influence of temperature on the fatigue behaviour of a toughened epoxy adhesive. Journal of Adhesion 2016;92:778–94. https://doi.org/10.1080/00218464.2015.1114927.

[54] Benelli A, Ciardiello R, Boursier Niutta C, Goglio L. Experimental and numerical characterization of adhesive joints with composite substrates by means of the Arcan test. Int J Adhes Adhes 2023;122:103321. https://doi.org/10.1016/J.IJADHADH.2022.103321.

[55] Ciampaglia A, Fiumarella D, Boursier Niutta C, Ciardiello R, Belingardi G. Impact response of an origami-shaped composite crash box: Experimental analysis and numerical optimization. Compos Struct 2021;256:113093. https://doi.org/10.1016/J.COMPSTRUCT.2020.113093.